The Journal of Chemical Physics

A complete quasiclassical map for the dynamics of interacting fermions

Cite as: J. Chem. Phys. **150**, 234112 (2019); https://doi.org/10.1063/1.5099987
Submitted: 13 April 2019 • Accepted: 31 May 2019 • Published Online: 19 June 2019

Amikam Levy, Wenjie Dou, Eran Rabani, et al.

AIP Publishing

The Journal of Chemical Physics ARTICLE scitation.org/journal/jcp

A complete quasiclassical map for the dynamics of interacting fermions

Cite as: J. Chem. Phys. 150, 234112 (2019); doi: 10.1063/1.5099987
Submitted: 13 April 2019 • Accepted: 31 May 2019 •
Published Online: 19 June 2019

Amikam Levy,[1,2,a] Wenjie Dou,[1] Eran Rabani,[1,2,3,b] and David T. Limmer[1,3,4,c]

AFFILIATIONS

[1] Department of Chemistry, University of California, Berkeley, Berkeley, California 94720, USA
[2] The Raymond and Beverly Sackler Center for Computational Molecular and Materials Science, Tel Aviv University, Tel Aviv 69978, Israel
[3] Materials Sciences Division, Lawrence Berkeley National Laboratory, Berkeley, California 94720, USA
[4] Kavli Energy NanoScience Institute, Berkeley, California 94720, USA

Note: This paper is part of a JCP Special Topic on Dynamics of Open Quantum Systems.
[a] **Electronic mail:** amikamlevy@gmail.com
[b] **Electronic mail:** eran.rabani@berkeley.edu
[c] **Electronic mail:** dlimmer@berkeley.edu

ABSTRACT

We present a strategy for mapping the dynamics of a fermionic quantum system to a set of classical dynamical variables. The approach is based on imposing the correspondence relation between the commutator and the Poisson bracket, preserving Heisenberg's equation of motion for one-body operators. In order to accommodate the effect of two-body terms, we further impose quantization on the spin-dependent occupation numbers in the classical equations of motion, with a parameter that is determined self-consistently. Expectation values for observables are taken with respect to an initial quasiclassical distribution that respects the original quantization of the occupation numbers. The proposed classical map becomes complete under the evolution of quadratic Hamiltonians and is extended for all even order observables. We show that the map provides an accurate description of the dynamics for an interacting quantum impurity model in the coulomb blockade regime, at both low and high temperatures. The numerical results are aided by a novel importance sampling scheme that employs a reference system to reduce significantly the sampling effort required to converge the classical calculations.

I. INTRODUCTION

Molecular simulation is an indispensable tool for understanding many-body quantum systems driven away from equilibrium. Describing the dynamics of molecular and mesoscopic electronics on time and length scales relevant to experiments, however, is challenging. In recent years, significant progress has been made by introducing numerically converged techniques, such as methods that rely on real-time diagrammatic sampling techniques,[1–9] wave function-based approaches such as numerical renormalization group techniques[10–12] and multilayer multiconfiguration methods,[13–15] or reduced and hierarchical density matrix approaches.[8,16] While significant progress has been made using these methods to understand the transport in various correlated scenarios,[17–19] their application to more realistic systems is still limited.

An alternative approach to these numerically converged techniques is based on approximate methods that are more flexible in describing realistic complex scenarios but often introduce simplifications leading to uncontrolled errors. Among the more popular methods are master equations (QME) and their generalizations[20–26] and approaches based on the nonequilibrium Green's function methods with specific closures for the self-energy.[27–32] More recently, quasiclassical mapping techniques[33–43] have been developed that cast the many-body quantum problem onto a set of classical dynamical variables and describe the transport in extended systems coupled to complex nonlinear environment, with varying coupling strengths. Such classical mapping procedures further admit the use of advanced sampling techniques of rare fluctuations[44] developed for classical molecular dynamics simulations.

Previous attempts to map the dynamics of fermionic systems onto a set of classical dynamical variables failed to reliably reproduce correlation effects, such as the Coulomb blockade staircase.[37,39–41] This is mainly due to the lack of quantization of the number operators in the classical map, leading to a continuous increase in the current with an increase in bias or gate voltage, in a quantum point-contact setup. Moreover, the description of the dynamics of observables that depend nonlinearly on a pair of creation and annihilation operators, for example, in those involved shot-noise measurements, has not received any attention. As shown below, a naïve and straightforward application of the classical maps to such observables leads to significant errors, even for the noninteracting model Hamiltonian, where the map generates the exact dynamics.

In this study, we develop a new strategy to map the dynamics of an open quantum system driven away from the equilibrium onto a set of classical dynamical variables. The method maps a pair of creation or annihilation fermionic operators to phase-space variables in Cartesian coordinates that satisfies a correspondence relation between the commutator and the Poisson brackets. In order to accommodate the effect of two-body terms (electron-electron interactions), we further impose quantization rules on the spin-dependent occupation numbers in the classical equations of motion, with parameter that is determined self-consistently. Combining this map with the initial value representation[45–47] that incorporates the discrete nature of quantum mechanics results in a robust description of the dynamics on diverse time scales, as illustrated for the Anderson impurity model[48] for a wide range of temperatures and the on-site electron-electron repulsion term. We further show that for quadratic Hamiltonians, higher order fermionic operators can be mapped accurately as a consequence of completeness, providing a framework to study the fluctuations and high order correlations within this mapping approach. Finally, we develop a reference sampling approach to reduce significantly the number of trajectories required to converge expectation values.

II. ANDERSON IMPURITY MODEL

For concreteness, throughout this manuscript, we consider the evolution of observables for the Anderson impurity model. This model is defined by the Hamiltonian $H = H_S + H_B + V$, where

$$\hat{H}_S = \sum_{\sigma=\uparrow,\downarrow} \varepsilon_\sigma \hat{d}_\sigma^\dagger \hat{d}_\sigma + U \hat{d}_\uparrow^\dagger \hat{d}_\uparrow \hat{d}_\downarrow^\dagger \hat{d}_\downarrow \tag{1}$$

describes the impurity (or dot), referred to simply as the "system Hamiltonian;"

$$\hat{H}_B = \sum_{\substack{\sigma=\uparrow,\downarrow \\ k\in \mathrm{L,R}}} \varepsilon_k \hat{c}_{k\sigma}^\dagger \hat{c}_{k\sigma} \tag{2}$$

describes the noninteracting fermionic baths (or leads); and

$$\hat{V} = \sum_{\substack{\sigma=\uparrow,\downarrow \\ k\in \mathrm{L,R}}} t_k \hat{d}_\sigma^\dagger \hat{c}_{k\sigma} + \mathrm{h.c.} \tag{3}$$

describes the hybridization between the system and the leads. Here, $d_\sigma^\dagger$ (d_σ) are the creation (annihilation) operators of an electron on the dot with spin $\sigma = \uparrow, \downarrow$ with a one-body energy ε_σ. U is the on-site Hubbard interaction, $\hat{c}_{k\sigma}^\dagger$ ($\hat{c}_{k\sigma}$) are the creation (annihilation) operators of an electron in mode k of the leads with energy ε_k, and t_k is the hybridization between the dot and mode k in the lead. The coupling to the quasicontinuous leads is modeled in the wide band limit. The spectral function of the left (ℓ = L) or right (ℓ = R) lead is

$$J_\ell(\varepsilon_k) = \frac{\Gamma_\ell}{\left(1 + e^{A(\varepsilon_k - B/2)}\right)\left(1 + e^{-A(\varepsilon_k + B/2)}\right)}, \tag{4}$$

where Γ_ℓ determines the coupling strength to the ℓ-lead, B is the width of the spectral function, and A determines the sharpness of the cutoff. The coupling t_k between the dot and the kth mode is expressed in terms of the spectral function as $t_{k\epsilon\ell} = \sqrt{J_\ell(\varepsilon_k)\Delta\varepsilon/2\pi}$, where $\Delta\varepsilon = 2\varepsilon_{\max}/(N_\ell/2 - 1)$ is the discretization of the leads energy spectrums, N_ℓ is the numbers of modes in the ℓ-lead, and $2\varepsilon_{\max}$ is the energy range in the leads. To model accurately the wide band limit, one should consider sufficiently large values for B such that the energy scale of the system is encompassed inside the spectrum of the leads and that the modes in the leads are dense enough, i.e., $\Delta\varepsilon$ is sufficiently small. In the simulations below, each lead consists of $N_\ell = 600$ modes, where half are with spin up and the other half are with spin down. For the parameters considered in this work, the number of bath modes is sufficiently large to converge the steady-state currents and populations on time scales shorter than the recurrence time. Throughout, we take $\hbar$, k_B, and the charge of the electron e to be 1.

To assess the accuracy and robustness of the quasiclassical mapping procedure, we focus on the Coulomb blockade effect that is manifested by a staircase structure of the current vs voltage, as shown in Fig. 1. When the bias voltage is not sufficiently large to overcome the on-site repulsion energy, only one conductance channel is open. When the bias becomes sufficiently large compared to U, an additional conducting channel opens up, and the current increases to its maximal value of a two-channel quantum point-contact. In Fig. 1, we show the results of two quasiclassical mapping procedures. The mapping approach that is isomorphic to quaternions [Li-Miller map (LMM)][39] provides an accurate description of the I-V characteristics at low and high bias voltages (V_{SD}) but

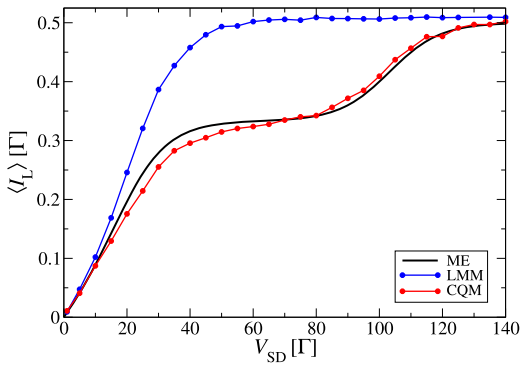

FIG. 1. The steady-state current from the left lead ($\langle I_L \rangle$) as a function of the bias voltage (V_{SD}). The black symbols are the results from the QME approach. The blue and red curves correspond to the LMM and CQM, respectively. Parameters used are $\Gamma = 2\Gamma_L = 2\Gamma_R = 1$, $\varepsilon_\uparrow = \varepsilon_\downarrow = 10\Gamma$, $T = 4\Gamma$, $U = 40\Gamma$, $\Delta_\sigma = 0.32$, $N_{\mathrm{tr}} = 3 \times 10^4$, and $\mu_L = -\mu_R = V/2$.

fails to reproduce the Coulomb blockade staircase. On the other hand, the current complete quasiclassical map (CQM) provides a qualitative description across all values of V_{SD}. In particular, it captures the staircase structure characteristic of the Coulomb Blockade effect. We will return to discuss the CQM results after we introduce the strategy of mapping quantum to classical degrees of freedom.

III. COMPLETE QUASICLASSICAL MAP (CQM)

For an operator $\hat{A}$, in the Hilbert space of the Anderson impurity model, the Heisenberg equation of motion reads

$$\frac{d\hat{A}}{dt} = i\left[\hat{H}_0, \hat{A}\right] + iU\left[\hat{n}_\uparrow, \hat{A}\right]\hat{n}_\downarrow + iU\hat{n}_\uparrow\left[\hat{n}_\downarrow, \hat{A}\right], \tag{5}$$

where $\hat{H}_0$,

$$\hat{H}_0 = \sum_{\sigma=\uparrow,\downarrow} \varepsilon_\sigma \hat{d}_\sigma^\dagger \hat{d}_\sigma + \sum_{\substack{\sigma=\uparrow,\downarrow \\ k\in L,R}} \varepsilon_k \hat{c}_{k\sigma}^\dagger \hat{c}_{k\sigma} + \sum_{\substack{\sigma=\uparrow,\downarrow \\ k\in L,R}} t_k \hat{d}_\sigma^\dagger \hat{c}_{k\sigma} + \text{h.c.} \tag{6}$$

is the one-body, noninteracting part of the Hamiltonian. We wish to find a map for $\hat{A}$ to a function of classical phase-space variables, $A[\vec{R}]$, that would preserve the dynamics $\langle \hat{A}(t) \rangle = \langle A(t) \rangle_c$, where $\langle \hat{A}(t) \rangle = \mathrm{Tr}\left(\hat{\rho}\hat{A}(t)\right)$ and

$$\langle A(t) \rangle_c = \int d\vec{R}\, \rho_0(\vec{R}) A[\vec{R}(t)] \tag{7}$$

is the classical expectation value with respect to the initial probability distribution ρ_0 of the total system. We do this in two parts. First, we construct a complete map for quadratic Hamiltonians, which is extendable to any even order operator and valid for noninteracting fermionic systems. Then, we propose a strategy for mapping Hamiltonians of higher order containing onsite Hubbard interactions. In all the simulations, the equations of motion are solved numerically using an adaptive Runge-Kutta method. The number of trajectories, N_{tr}, used to converge the results is specified below for each case study. For the steady-state results, additional time averaging is considered.

A. Noninteracting fermions

We first consider the case of noninteracting fermions, $U = 0$, described by a Hamiltonian that depends quadratically on the creation and annihilation operators, $\hat{H}_0$. To reproduce the dynamics of the expectation value of quadratic operators under the evolution describe in Eq. (5), we require the following:

(a) For any quadratic operator $\hat{A}$, and its classical counterpart A, the commutator and the Poisson bracket satisfies the correspondence relation $i\left[\hat{H}_0, \hat{A}\right] = \{A, H_0\}$.
(b) For any quadratic expectation value, the initial probability distribution ρ_0 must satisfy $\langle \hat{A}(0) \rangle = \langle A(0) \rangle_c$ and respect the quantum discrete nature of the occupations.

It is straightforward to show that condition (a) is satisfied by mapping a pair of creation and annihilation operators to a phase space of conjugated variables, $\vec{R} = (x, p_x, y, p_y)$, as

$$\begin{aligned}
\hat{a}_n^\dagger \hat{a}_n &\mapsto x_n p_{y,n} - y_n p_{x,n}, \\
\hat{a}_n^\dagger \hat{a}_m &\underset{m\neq n}{\mapsto} \frac{1}{2}\left[i(x_n p_{x,m} - p_{x,n}x_m + y_n p_{y,m} - p_{y,n}y_m)\right. \\
&\quad \left. + (x_n p_{y,m} - p_{x,n}y_m + x_m p_{y,n} - p_{x,m}y_n)\right], \\
\hat{a}_n^\dagger \hat{a}_m^\dagger &\mapsto \frac{1}{2}\left[i(x_n p_{x,m} - p_{x,n}x_m - y_n p_{y,m} + p_{y,n}y_m)\right. \\
&\quad \left. - (x_n p_{y,m} - p_{x,n}y_m - x_m p_{y,n} + p_{x,m}y_n)\right], \\
\hat{a}_n \hat{a}_m &\mapsto \frac{1}{2}\left[i(x_n p_{x,m} - p_{x,n}x_m - y_n p_{y,m} + p_{y,n}y_m)\right. \\
&\quad \left. + (x_n p_{y,m} - p_{x,n}y_m - x_m p_{y,n} + p_{x,m}y_n)\right].
\end{aligned} \tag{8}$$

This identifies positions, (x, y), and their conjugate momenta, (p_x, p_y), and the Poisson bracket can be used to check that this map returns the quantum commutator of any pair of quadratic creation/annihilation operators. Because any quadratic Hamiltonian with a set of quadratic operators constitutes a closed Lie algebra of quadratic operators, condition (a) insures a loyal representation of the dynamics in terms of Hamilton's equations. We note in passing that we subtracted 1/2 from the classical map of $\hat{n}_i \equiv \hat{a}_i^\dagger \hat{a}_i$ to include a Langer-like correction.[49]

For leads that are in thermal equilibrium and the uncorrelated initial state, condition (b) can be satisfied by setting the initial occupation of each mode in the left and right leads to a value 0 or 1 such that the expectation value, averaged over the set of initial conditions, satisfies the Fermi-Dirac distribution.[37] Operationally, we choose a random number $\xi_{k\sigma} \in [0, 1]$ and then select the occupation of mode $k\sigma$ of the ℓ-lead according to

$$n_{k\sigma} = \begin{cases} 0 & \xi_{k\sigma} > \left(1 + e^{\beta_\ell(\varepsilon_k - \mu_\ell)}\right)^{-1} \\ 1 & \xi_{k\sigma} \leq \left(1 + e^{\beta_\ell(\varepsilon_k - \mu_\ell)}\right)^{-1}, \end{cases} \tag{9}$$

where $\beta_\ell = 1/k_B T_\ell$ and μ_l are the inverse temperature times Boltzmann's constant and chemical potential of the ℓ-lead, respectively. The Cartesian coordinates are then sampled according to[40]

$$\begin{aligned}
x_{k\sigma} &= \cos(\theta_{k\sigma}), \quad & p_{x,n\sigma} &= -n_{k\sigma}\sin(\theta_{k\sigma}), \\
y_{k\sigma} &= \sin(\theta_{k\sigma}), \quad & p_{y,n\sigma} &= n_{k\sigma}\cos(\theta_{k\sigma}),
\end{aligned} \tag{10}$$

where $\theta_{k\sigma}$ is chosen randomly in the interval $[0, 2\pi]$ and $n_{k\sigma} = x_{k\sigma}p_{y,k\sigma} - y_{k\sigma}p_{x,k\sigma}$ satisfies Eq. (9), resulting in $\langle \hat{n}_{k\sigma} \rangle = \langle n_{k\sigma} \rangle_c = (1 + \exp[\beta_\ell(\varepsilon_k - \mu_\ell)])^{-1}$ at the initial time. By construction, the expectation value at the initial time is $\langle a_n^\dagger a_m \rangle_c = \langle a_n^\dagger a_m^\dagger \rangle_c = \langle a_n a_m \rangle_c = 0$, as expected for averages taken with respect to uncorrelated thermal distribution. The sampling choice in Eq. (10) is not unique, but it does provide an efficient averaging of the expectation values with respect to the number of trajectories.[40] In a similar manner, one can set the initial occupation of the dot.

Comparing the proposed CQM given by Eq. (8) to the LMM, we find that the mappings of the diagonal term $\hat{a}_n^\dagger \hat{a}_n$ and of the linear combination $\hat{a}_n^\dagger \hat{a}_m^\dagger + \hat{a}_m^\dagger \hat{a}_n^\dagger$ are identical in both maps, but the remaining terms in Eq. (8) cannot be expressed using the LMM (see Appendix A for more information). This leads to the Hamiltonian

being expressed identically in both maps,

$$H_0 = \sum_{\sigma=\uparrow,\downarrow} \varepsilon_\sigma \left(x_\sigma p_{y,\sigma} - y_\sigma p_{x,\sigma}\right) + \sum_{\substack{\sigma=\uparrow,\downarrow \\ k\in L,R}} \varepsilon_k \left(x_{k\sigma} p_{y,k\sigma} - y_{k\sigma} p_{x,k\sigma}\right) + \sum_{\substack{\sigma=\uparrow,\downarrow \\ k\in L,R}} t_k \left(x_\sigma p_{y,k\sigma} - y_\sigma p_{x,k\sigma} + x_{k\sigma} p_{y,\sigma} - y_{k\sigma} p_{x,\sigma}\right). \tag{11}$$

For this noninteracting Hamiltonian, mapping H_0 and then deriving Hamilton's equations of motion for the phase space variables are identical to deriving Heisenberg's equation of motion for the bilinear operators and then mapping the results using Eq. (8).

We can also map other quadratic observables, such as the current from the left lead

$$\hat{I}_L = -\frac{d}{dt} \sum_{\substack{\sigma=\uparrow,\downarrow \\ k\in L}} \hat{c}^\dagger_{k\sigma} \hat{c}_{k\sigma} \mapsto \sum_{\substack{\sigma=\uparrow,\downarrow \\ k\in L}} t_k \left(y_\sigma p_{y,k\sigma} - p_{y,\sigma} y_{k\sigma} + x_\sigma p_{x,k\sigma} - p_{x,\sigma} x_{k\sigma}\right). \tag{12}$$

As a diagonal term, the above form is also identical to the expression obtained by the LMM.[40] In the upper panel of Fig. 2, we compare the results for the left current generated by the CQM (which in this case are equivalent to the LMM) with exact quantum mechanical results for a noninteracting model Hamiltonian. As expected, the agreement between the CQM (or the LMM) and exact quantum mechanical results is excellent. In Sec. III B, we show that for the CQM these results can be extended to higher-order operators.

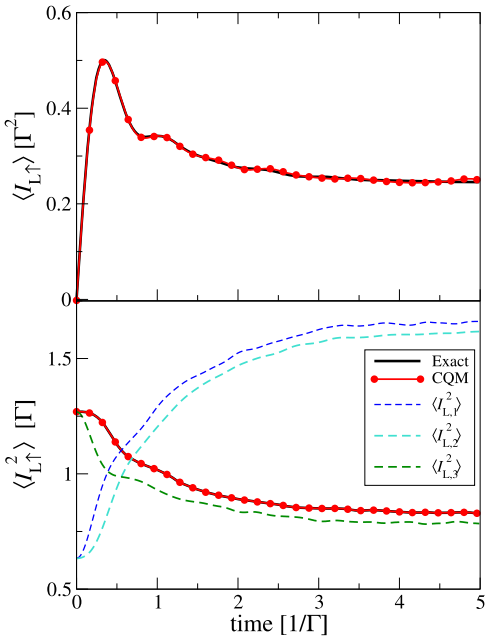

FIG. 2. Upper panel: the average left current for spin up ($\langle I_{L\uparrow}(t) \rangle$) as a function of time for a noninteracting model Hamiltonian. The solid black line represents the exact quantum mechanical result[37] and the red symbols are the result of the CQM. Lower panel: the average left current squared for spin up ($\langle I^2_{L\uparrow}(t) \rangle$) as a function of time. In addition to the exact quantum mechanical (solid black curve) and CQM (red symbols) results, we also show the individual terms $\langle I^2_{L,1}(t) \rangle$ (blue), $\langle I^2_{L,2}(t) \rangle$ (cyan), and $\langle I^2_{L,3}(t) \rangle$ (green). Parameters used are $\Gamma = 2\Gamma_L = 2\Gamma_R = 1$, $\varepsilon_\uparrow = \varepsilon_\downarrow = -\Gamma$, $T = \frac{\Gamma}{5}$, $U = 0$, $N_{tr} = 10^5$, and $\mu_L = -\mu_R = 6\Gamma$.

B. Higher order operators

Mapping higher order operators, operators that involve more than one pair of creation/annihilation operators, is more difficult due to the nonlocal character of fermions arising from their exclusion statistics. Ignoring the fermionic nature does not seem to make any significant difference for a single pair of creation/annihilation operators,[37,40] but for higher order operators, the anticommutation of the creation/annihilation fermionic operators plays a significant role and describing quantum fluctuations such as shot noise requires a careful consideration of this effect.

For example, consider a map for the operator $\hat{A} = a^\dagger_n a_m a^\dagger_m a_k$. Using the anticommutation nature of $\{\hat{a}^\dagger_n, \hat{a}_n\} = 1$, we can express the expectation value of $\hat{A}$ using four different terms that are identical quantum mechanically, but differ when mapped onto classical phase space variables. Specifically, expanding $\langle \hat{A} \rangle$

$$\begin{aligned} \left\langle \hat{a}^\dagger_n \hat{a}_m \hat{a}^\dagger_m \hat{a}_k \right\rangle = C_1 \left\langle \left(\hat{a}^\dagger_n \hat{a}_m\right)\left(\hat{a}^\dagger_m \hat{a}_k\right) \right\rangle + C_2 \Big\langle \left(\hat{a}^\dagger_n \hat{a}_k\right) \\ - \left(\hat{a}^\dagger_n \hat{a}^\dagger_m\right)\left(\hat{a}_m \hat{a}_k\right) \Big\rangle + C_3 \left\langle \left(\hat{a}^\dagger_n \hat{a}_k\right)\left(\hat{a}_m \hat{a}^\dagger_m\right) \right\rangle \\ + C_4 \left\langle \delta_{nk}\left(\hat{a}_m \hat{a}^\dagger_m\right) - \left(\hat{a}_k \hat{a}_m\right)\left(\hat{a}^\dagger_m \hat{a}^\dagger_n\right) \right\rangle, \end{aligned} \tag{13}$$

we find that there are four unique combinations of operators, which generically have coefficients, C_i. To determine the best choice of C_i, we impose conditions (a) and (b) of Sec. III A on the time evolution of $\hat{A}$ and require that the time evolution of $\hat{A}$ be exact for a quadratic Hamiltonian, i.e., that $i[\hat{H}, \hat{A}] = \{A, H\}$ and that $\langle \hat{A}(0) \rangle = \langle A(0) \rangle_c$. For an uncorrelated initial thermal state, the values that satisfy these conditions are $C_1 = 1$, $C_2 = -1$, $C_3 = 1$, and $C_4 = 0$. Note that Eq. (13) contains pairs of creation or annihilation operators ($a^\dagger_n a^\dagger_m$ or $a_n a_m$), which cannot be described within the LMM.

Applying this procedure to the second moment of the left current for the noninteracting Hamiltonian yields a simple expression for $\langle \hat{I}^2_L \rangle = \langle \hat{I}^2_{L,1} \rangle - \langle \hat{I}^2_{L,2} \rangle + \langle \hat{I}^2_{L,3} \rangle$, where

$$\begin{aligned} \left\langle \hat{I}^2_{L,1} \right\rangle &= \sum_{\substack{\sigma=\uparrow,\downarrow \\ j,k\in L}} t_j t_k \left\langle \left(\hat{c}^\dagger_{j\sigma} \hat{d}_\sigma\right)\left(\hat{d}^\dagger_\sigma \hat{c}_{k\sigma}\right) + \left(\hat{d}^\dagger_\sigma \hat{c}_{j\sigma}\right)\left(\hat{c}^\dagger_{k\sigma} \hat{d}_\sigma\right) \right\rangle, \\ \left\langle \hat{I}^2_{L,2} \right\rangle &= \sum_{\substack{\sigma=\uparrow,\downarrow \\ j,k\in L}} t_j t_k \Big\langle \left(\hat{c}^\dagger_{j\sigma} \hat{c}_{k\sigma}\right) - \left(\hat{c}^\dagger_{j\sigma} \hat{d}^\dagger_\sigma\right)\left(\hat{d}_\sigma \hat{c}_{k\sigma}\right) \\ &\quad + \delta_{jk}\left(\hat{d}^\dagger_\sigma \hat{d}_\sigma\right) - \left(\hat{d}^\dagger_\sigma \hat{c}^\dagger_{k\sigma}\right)\left(\hat{c}_{j\sigma} \hat{d}_\sigma\right) \Big\rangle, \\ \left\langle \hat{I}^2_{L,3} \right\rangle &= \sum_{\substack{\sigma=\uparrow,\downarrow \\ j,k\in L}} t_j t_k \left\langle \left(\hat{c}^\dagger_{j\sigma} \hat{c}_{k\sigma}\right)\left(\hat{d}_\sigma \hat{d}^\dagger_\sigma\right) + \left(\hat{d}^\dagger_\sigma \hat{d}_\sigma\right)\left(\hat{c}_{j\sigma} \hat{c}^\dagger_{k\sigma}\right) \right\rangle. \end{aligned} \tag{14}$$

As can be shown explicitly, this mapping of the second moment of the left current operator satisfies both conditions (a) and (b).

In the bottom panel of Fig. 2, we show the time evolution of $\langle \hat{I}^2_L \rangle$ for a quadratic Hamiltonian where $U = 0$. The agreement between the exact quantum mechanical result and the CQM is excellent. We also plot the individual terms $\langle \hat{I}^2_{L,1} \rangle$, $\langle \hat{I}^2_{L,2} \rangle$, and $\langle \hat{I}^2_{L,3} \rangle$ (dashed lines). Only the proper combination of all three terms yields an accurate description of $\langle \hat{I}^2_L \rangle$. We note that the LMM can only be used to map the first term, but not the other two that contribute to $\langle \hat{I}^2_L \rangle$.

C. Interacting fermions

The on-site interaction, $U\hat{n}_\uparrow\hat{n}_\downarrow$, that manifest the Coulomb blockade effect, is a four index term that is outside the space defined by the CQM. In order to account for this two-body interaction term, we map the two terms proportional to U in Eq. (5) according to

$$\begin{aligned} iU\left[\hat{n}_\uparrow, \hat{A}\right]\hat{n}_\downarrow &\mapsto U\{A, n_\uparrow\}\theta(n_\downarrow - \Delta_\downarrow), \\ iU\hat{n}_\uparrow\left[\hat{n}_\downarrow, \hat{A}\right] &\mapsto U\{A, n_\downarrow\}\theta(n_\uparrow - \Delta_\uparrow), \end{aligned} \tag{15}$$

where θ is the Heaviside step function. The idea behind this choice is that the term $U\hat{n}_\uparrow\hat{n}_\downarrow$ contributes to the dynamics only when both electrons with spin up and spin down occupy the site. Classically, the occupation number admits a continuous value, which implies that the Hubbard term can become significant for fractional populations of the two spin-channels. Much like a mean-field approximation, these fraction contributions of the Hubbard term will smear the Coulomb blockade effect. By introducing the step function, we impose that contributions to the dynamics from the Hubbard term arise only in trajectories for which $n_{\uparrow(\downarrow)} > \Delta_{\uparrow(\downarrow)}$. The parameter $\Delta_{\uparrow(\downarrow)}$ is determined according to the distribution of $n_{\uparrow(\downarrow)}$ and will be discussed in detail below. We note that the classical expression in Eq. (15) neglects explicitly derivatives of the step function that would come from an effective Hamiltonian that governs the mapped dynamics (see Appendix B for more details). As such, the equations of motion do not conserve the energy associated with this effective Hamiltonian or the norm of phase space. However, we have checked that over the time scales considered here, the drift in the effective Hamiltonian is small and accumulates to less than 0.05% of the total effective energy as the system relaxes to steady-state (see Appendix B).

Considering the Anderson impurity model, the equations of motion for the Cartesian variables for the lead degrees of freedom are

$$\begin{aligned} \dot{x}_{j\sigma} &= -\varepsilon_j y_{j\sigma} - t_j y_\sigma, \\ \dot{y}_{j\sigma} &= \varepsilon_j x_{j\sigma} + t_j x_\sigma, \\ \dot{p}_{x,j\sigma} &= -\varepsilon_j p_{y,j\sigma} - t_j p_{y,\sigma}, \\ \dot{p}_{y,j\sigma} &= \varepsilon_j p_{x,j\sigma} + t_j p_{x,\sigma}, \end{aligned} \tag{16}$$

and those for the system's degrees of freedom are

$$\begin{aligned} \dot{x}_\sigma &= -\varepsilon_\sigma y_\sigma - \sum_{k\in L,R} t_k y_{k\sigma} - U y_\sigma \theta(n_{\bar{\sigma}} - \Delta_{\bar{\sigma}}), \\ \dot{y}_\sigma &= \varepsilon_\sigma x_\sigma + \sum_{k\in L,R} t_k x_{k\sigma} + U x_\sigma \theta(n_{\bar{\sigma}} - \Delta_{\bar{\sigma}}), \\ \dot{p}_{x,\sigma} &= -\varepsilon_\sigma p_{y,\sigma} - \sum_{k\in L,R} t_k p_{y,k\sigma} - U p_{y,\sigma} \theta(n_{\bar{\sigma}} - \Delta_{\bar{\sigma}}), \\ \dot{p}_{y,\sigma} &= \varepsilon_\sigma p_{x,\sigma} + \sum_{k\in L,R} t_k p_{x,k\sigma} + U p_{x,\sigma} \theta(n_{\bar{\sigma}} - \Delta_{\bar{\sigma}}), \end{aligned} \tag{17}$$

where $\bar{\sigma} = \downarrow, \uparrow$ is the opposite spin to $\sigma = \uparrow, \downarrow$.

In Fig. 1, we plot the I-V curve obtained by the CQM and compare it to the QME in Ref. 50 and to the results obtained by the LMM. We consider the limit of the weak system-bath coupling and high temperature where the QME provides a good approximation for the dynamics of the system. The LMM provides a good description of the I-V characteristics at low and high bias voltages, but it fails to capture the staircase structure reminiscent of the Coulomb blockade. The CQM reproduces the QME results quantitatively; specifically, it captures the staircase structure due to the Coulomb blockade effect. In this high temperature regime, the agreement between the CQM and the quantum mechanical results is observed for a wide range of the onsite Hubbard repulsion term and also for the quantum dot population.

Next, we consider a regime where the QME breaks down, namely, the low temperature regime. For simplicity, we focus on the equilibrium case where $\mu_L = \mu_R = 0$. In this regime, solutions for the population as functions of the gate voltage ($\varepsilon = \varepsilon_\uparrow = \varepsilon_\downarrow$) are readily available using the numerical renormalization group (NRG) technique.[51] In the left panel of Fig. 3, we plot the quantum dot total population ($\langle n_\uparrow + n_\downarrow \rangle$) as a function of the gate voltage. The NRG results show a staircase shape which is a manifestation of the Coulomb blockade effect. The CQM agrees quantitatively with the NRG results over a wide range of gate voltages. Specifically, it captures both the position of the blockade as well as its width. The QME approach, however, captures only the position of the resonances; the broadening of the transitions is missing completely. This qualitative difference between the CQM and QME approaches signifies the advantages of the quasiclassical mapping techniques over the commonly used QME approach for a broad range of temperatures.

The mapping of the Hubbard term in Eq. (15) introduces a parameter, Δ_σ, which is determined self-consistently. The basic idea is simple: the occupation of the dot n_σ outside the commutator is substituted with a step function $\theta(n_\sigma - \Delta_\sigma)$ for the interaction term only to mimic the quantization of the population. To fix Δ_σ, we consider a set of parameters where the value of the steady state population $\langle \hat{n}_\sigma \rangle = 1/2$ (high bias or particle-hole symmetric point for the current model) and determine self-consistently the value of Δ_σ such that classically $\langle \theta(n_\sigma - \Delta_\sigma) \rangle = 1/2$. Then, for $n_\sigma > \Delta_\sigma$, the dot is considered classically occupied and the interaction term influences the dynamics.

For the results shown in Fig. 3, we use a single value for $\Delta_\sigma = 0.18$, determined by considering the particle-hole symmetric point, where $\varepsilon_\uparrow = \varepsilon_\downarrow = -U/2 = -5\Gamma$. At the symmetric point, the steady state value of the average dot populations is $\langle \hat{n}_\sigma \rangle = 1/2$. We then set Δ_σ to the median of the distribution of n_σ (see Appendix C). This ensures that the Hubbard terms in Eq. (15) are significant only when $n_\sigma > \Delta_\sigma$. In the right panel of Fig. 3, we show the results obtained

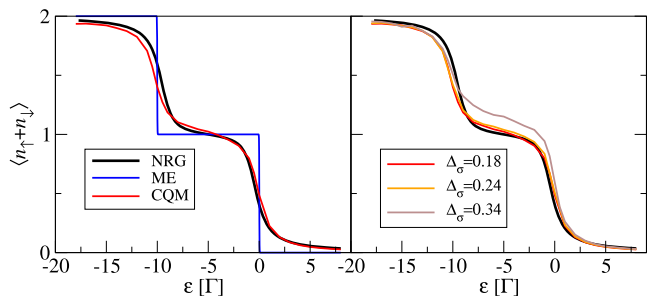

FIG. 3. Left panel: the steady-state quantum dot population as a function of the gate voltage $\varepsilon = \varepsilon_\uparrow = \varepsilon_\downarrow$ under equilibrium conditions ($\mu_L = \mu_R = 0$). Right panel: the dependence of the steady-state dot population on the choice of the value of Δ_σ [cf., Eq. (15)]. Parameters used are $\Gamma = 2\Gamma_L = 2\Gamma_R = 1$, $T = \Gamma/100$, $U = 10\Gamma$, $N_{tr} = 3 \times 10^4$, and, for the left panel, $\Delta_\sigma = 0.18$.

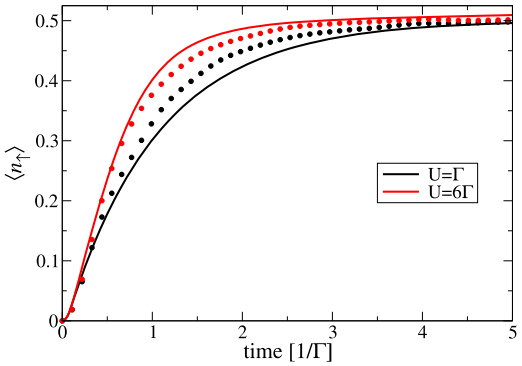

FIG. 4. Comparison of the dot population ($\langle n_\uparrow + n_\downarrow \rangle$) derived from the memory-kernel formalism[7] (solid lines) and the CQM approach (dot symbols) for an initially unoccupied dot for two values of the interaction energy ($U = \Gamma$ and $U = 6\Gamma$). Parameters used are $\Gamma = 2\Gamma_L = 2\Gamma_R = 1$, $T = \Gamma$, $\mu_L = -\mu_R = \Gamma/2$, $\varepsilon_\uparrow = \varepsilon_\downarrow = -U/2$, and $N_{tr} = 6 \times 10^4$, and for the CQM results, $\Delta_\sigma = 0.24$ for $U = 6\Gamma$ and $\Delta_\sigma = 0.31$ for $U = \Gamma$.

for the total dot occupation for different values of Δ_σ. Only 3 iterations are required to converge the results for Δ_σ within the noise level of our simulations. To do this, we start with an initial guess of $\Delta_\sigma = 0.34$. In the next iteration, we set Δ_σ to the new median of the distribution of n_σ, in this case $\Delta_\sigma = 0.24$. We then repeat this procedure until convergence of the median (only one more iteration is required in this present case). We then use the value of Δ_σ found for the symmetric point for other model parameters. The results in the right panel of Fig. 3 clearly indicate that the average dot population is not very sensitive to small variations in the value of Δ_σ, but the converged results provide the best agreement with the NRG calculations.

The agreement between the CQM and the quantum mechanical results are not limited to steady-state properties. In fact, our mapping also captures quantitatively the hallmarks of the Coulomb blockade in the relaxation toward the steady state. Shown in Fig. 4 is the time dependence of the dot occupation for two different values of U, with a bias voltage of $V_{SD} = \mu_L - \mu_R = \Gamma$ and temperature $T = \Gamma$. Here, we compare the CQM to numerically converged real-time stochastically sampled diagrammatic techniques applied within the reduced density matrix formalism.[7] For both values of U, we find that the full time dependence is in good agreement with the numerically converged data. In each case, the dot population increases monotonically and the time scales required to reach the long time limit are comparable.

IV. REFERENCE DYNAMICS FOR STATISTICAL CONVERGENCE

When evaluating the classical expected value Eq. (7), the integral over the initial distribution is replaced by averaging over different initial configurations of the leads that satisfy the Fermi-Dirac distribution. For a large number of initial conditions, N_{tr}, the procedure converges to the desired distribution and to the exact expectation value. However, the low dimensional nearly harmonic system generically requires a large number of initial conditions to statistically converge the result. To reduce the number of initial conditions for a given statistical error, we introduce a reference system whose expectation value can be determined exactly and inexpensively. Specifically, the expectation value of an observable A is calculated according to

$$\langle A \rangle = \langle A_r - A_r + A \rangle = \bar{A}_r + \langle \Delta A \rangle, \tag{18}$$

where A_r is an observable used as the reference and $\bar{A}_r$ is the exact expectation value of A_r evaluated using a different inexpensive method. In the limit $N_{tr} \to \infty$, we have $\langle A_r \rangle \to \bar{A}_r$ and $\langle A \rangle$ will approach the real expectation value. However, for a finite N_{tr}, and a smart choice of A_r, one can reduce significantly the statistical error of this estimator. This is clarified by considering the variance using the reference system

$$\mathrm{Var}(\Delta A) = \mathrm{Var}(A) + \mathrm{Var}(A_r) - 2\mathrm{Cov}(A, A_r). \tag{19}$$

If A and A_r are correlated, it is possible to have $\mathrm{Var}(\Delta A) < \mathrm{Var}(A)$. As we are now propagating both A and A_r, to reduce the computational effort, we desire that

$$\frac{\mathrm{Var}(\Delta A)}{\mathrm{Var}(A)} < \frac{1}{2}. \tag{20}$$

Given that the sample variance reduces as $1/N_{tr}$, to obtain computational superiority, the ratio in Eq. (20) is bounded by 1/2. However, improvement in the computational effort can already be seen for ratios that are above this factor since typically propagation of the reference system is not as costly as of the system of interest. Noninteracting or mean-field Hamiltonians that can be solved analytically serve as examples of reference systems that can reduce noise for the dynamics of interacting systems. Other possibilities include considering dynamics that are generated from some effective Hamiltonian with the same initial configurations.

Shown in Fig. 5 are two examples, one in which the reference system method works well and one in which it fails. On the left panel, we plot the ratio of the variances of the left current with spin up as a function of time, and on the right, we plot the corresponding currents. The reference considered here is the current calculated for noninteracting systems where an exact solution can be obtained by direct diagonalization of the single-particle Hamiltonian. We see that when the reference current, $\bar{I}_r$, becomes very different from the real current, $\bar{I}_r + \langle \Delta I \rangle$ (for $U = 6\Gamma$ in the figure), the ratio of the

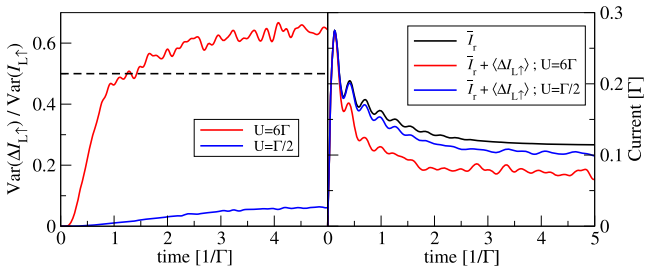

FIG. 5. Left panel: the ratio of the variances of the left currents for spin up as a function of time. The red line is for $U = 6\Gamma$ and the blue for $U = \Gamma/2$. Computational superiority is observed below the threshold ratio 1/2 noted by the black dashed line. Right panel: the black line is the exact reference current ($U = 0$), and the red and blue line are the currents obtained using a reference system for $U = 6\Gamma$ and $U = \Gamma$, respectively. The parameters are $\Gamma = 2\Gamma_L = 2\Gamma_R = 1$, $T = 0.5\Gamma$, $\varepsilon_\uparrow = \varepsilon_\downarrow = 2\Gamma$, $N_{tr} = 3 \times 10^4$, and $\mu_L = -\mu_R = 2\Gamma$.

variances at steady-state exceeds its bound 1/2. However, when the reference and the real currents are proximate but still quite different (for $U = \Gamma/2$ in the figure), we see that the ratio of the variances is reduced significantly as a consequence of correlations between the trajectories of the currents.

We note that for the parameter regime where the reference and real currents almost coincide, the fluctuations drastically decreased, and the ratio of the variances at the steady state reached as low as $\sim 10^{-4}$. This implies that for a fixed statistical convergence threshold, the number of initial conditions decreases by two orders of magnitude since each estimate is statistically independent. One can also note that at short times, the reference system always reduces the fluctuations significantly. The reason is that we used an uncorrelated initial condition and thus the short time behavior is set by $\sim\Gamma^{-1}$. It takes a certain amount of time for correlations to build up and for the interacting part in the Hamiltonian to influence the dynamics, yielding a statistical benefit for short times even when the steady-state result is far from the noninteracting limit.

The idea of using a reference system can be extended beyond the description above. For example, if one wishes to calculate the current as function of U, one can start the evaluation for small U and increase it "adiabatically." For each calculation of the current, the previous current (with smaller U) can be used as the reference system. Of course, the exact term in Eq. (18) is no longer exact and carries with it some error, but this can still be beneficial, as trajectories of the different currents are likely to be correlated given that the change in U is small.

V. CONCLUSIONS

We have presented a quasiclassical method to simulate nonequilibrium dynamics of interacting fermions. We have constructed this map using the correspondence relation between the commutator and the Poisson bracket, in order to preserve Heisenberg's equation of motion for one-body operators. We have shown that this classical map is complete for quadratic expectation values under quadratic Hamiltonians and it can be extended to higher moments accurately. This feature makes the study of fluctuations and higher-order correlations accessible.

For interacting systems, the dynamics is approximated by mapping the equation of motion and enforcing a quantization rule that determines for which values of n_σ the dynamics is influenced by the Hubbard term. This, together with a quasiclassical initial distribution, provides a quantitative agreement with other methods in regimes where those other methods are known to be accurate. Thus, a quantitative description of nonequilibrium currents in the Anderson model, including their steady-state behavior as illustrated by the presence of the Coulomb blockade, their fluctuations as encodes in the second moment of the current, and the relaxation of each to their steady state, can be obtained.

We have also shown a way to enhance the statistical convergence of this method by introducing a reference system, whose dynamics can be computed exactly, and averaging the difference between the reference system and the system of interest. Provided that the reference system is correlated with the system of interest, fluctuations are reduced in the averaging procedure, and we have shown that this can increase the computational efficiency by up to 2 orders of magnitude over naïve sampling. Together, these results make the quasiclassical method appealing for studying nonequilibrium phenomena in complex chemical systems. Indeed, realistic systems of molecular junctions routinely operate at low effective temperatures, and finite interaction strengths render other low scaling approximate approaches inaccurate. The method we have presented here is capable of probing these regimes, at a small computational cost that scales linearly in the system degrees of freedom. This should enable studies in correlated transport behavior in high dimensional, molecular systems, far from equilibrium.

ACKNOWLEDGMENTS

This work was supported by the U.S. Department of Energy, Office of Basic Energy Sciences, Materials Sciences and Engineering Division, under Contract No. DEAC02-05-CH11231 within the Physical Chemistry of Inorganic Nanostructures Program (Grant No. KC3103). The authors thank Lyran Kidon for the stimulated discussions.

APPENDIX A: RELATION TO QUATERNION MAPS

The LMM[39,40] is based on expressing the fermionic creation and annihilation operators in terms of a set of quaternions

$$\begin{aligned}\hat{a}^\dagger &= \frac{1}{2}(\sqrt{-1}\,\hat{\mathrm{i}} - \hat{\mathrm{j}}),\\ \hat{a} &= \frac{1}{2}(\sqrt{-1}\,\hat{\mathrm{i}} + \hat{\mathrm{j}}).\end{aligned} \tag{A1}$$

The quaternions operators $\hat{\mathrm{i}}, \hat{\mathrm{j}}$, and $\hat{\mathrm{k}}$ satisfy the anticommutation relation

$$\begin{gathered}\hat{\mathrm{i}}\hat{\mathrm{j}} = -\hat{\mathrm{j}}\hat{\mathrm{i}} = \hat{\mathrm{k}}, \quad \hat{\mathrm{j}}\hat{\mathrm{k}} = -\hat{\mathrm{k}}\hat{\mathrm{j}} = \hat{\mathrm{i}}, \quad \hat{\mathrm{k}}\hat{\mathrm{i}} = -\hat{\mathrm{i}}\hat{\mathrm{k}} = \hat{\mathrm{j}},\\ \hat{\mathrm{i}}^2 = \hat{\mathrm{j}}^2 = \hat{\mathrm{k}}^2 = -1.\end{gathered} \tag{A2}$$

Using the relations in Eqs. (A1) and (A2), quadratic creation and annihilation operators can be expressed as

$$\begin{aligned}\hat{a}_n^\dagger \hat{a}_n &= \frac{1}{2} + \frac{\sqrt{-1}}{2}\hat{\mathrm{i}}_n\hat{\mathrm{j}}_n,\\ \hat{a}_n^\dagger \hat{a}_m &= \frac{1}{4}\left(-\hat{\mathrm{i}}_n\hat{\mathrm{i}}_m - \hat{\mathrm{j}}_n\hat{\mathrm{j}}_m + \sqrt{-1}\left(\hat{\mathrm{i}}_n\hat{\mathrm{j}}_m + \hat{\mathrm{i}}_m\hat{\mathrm{j}}_n\right)\right),\\ \hat{a}_n^\dagger \hat{a}_m^\dagger &= \frac{1}{4}\left(-\hat{\mathrm{i}}_n\hat{\mathrm{i}}_m + \hat{\mathrm{j}}_n\hat{\mathrm{j}}_m - \sqrt{-1}\left(\hat{\mathrm{i}}_n\hat{\mathrm{j}}_m - \hat{\mathrm{i}}_m\hat{\mathrm{j}}_n\right)\right),\\ \hat{a}_n\hat{a}_m &= \frac{1}{4}\left(-\hat{\mathrm{i}}_n\hat{\mathrm{i}}_m + \hat{\mathrm{j}}_n\hat{\mathrm{j}}_m + \sqrt{-1}\left(\hat{\mathrm{i}}_n\hat{\mathrm{j}}_m - \hat{\mathrm{i}}_m\hat{\mathrm{j}}_n\right)\right).\end{aligned} \tag{A3}$$

The commutation relation of two elementary quaternions are then mapped to a cross product of vectors in phase space,

$$\sqrt{\frac{-1}{2}}\,\hat{\mathrm{i}} \to \mathbf{r} = \begin{pmatrix} x \\ y \end{pmatrix}, \quad \sqrt{\frac{1}{2}}\,\hat{\mathrm{j}} \to \mathbf{p} = \begin{pmatrix} p_x \\ p_y \end{pmatrix}. \tag{A4}$$

The CQM replaces the map in Eq. (A4) with

$$\sqrt{\frac{\sqrt{-1}}{2}}\,\hat{\mathrm{i}} \to u = \begin{pmatrix} x \\ p_x \end{pmatrix}, \quad \sqrt{\frac{\sqrt{-1}}{2}}\,\hat{\mathrm{j}} \to v = \begin{pmatrix} y \\ p_y \end{pmatrix}. \tag{A5}$$

This choice implies that

$$\frac{\sqrt{-1}}{2}\hat{i}_n\hat{j}_m \to u_n \times v_m = x_m p_{ym} - p_{xn} y_m,$$
$$\frac{\sqrt{-1}}{2}\hat{i}_n\hat{i}_m \to u_n \times u_m = x_m p_{xm} - p_{xn} x_m, \quad \forall n \neq m, \tag{A6}$$
$$\frac{\sqrt{-1}}{2}\hat{j}_n\hat{j}_m \to v_n \times v_m = y_m p_{ym} - p_{yn} y_m, \quad \forall n \neq m,$$

and $\frac{\sqrt{-1}}{2}\hat{i}\hat{i} = \frac{\sqrt{-1}}{2}\hat{j}\hat{j} = -\frac{\sqrt{-1}}{2}$ for $n = m$. The LMM given by Eq. (A4) can be used to map the terms $\hat{a}_n^\dagger\hat{a}_n$ and $\hat{a}_n^\dagger\hat{a}_m + \hat{a}_m^\dagger\hat{a}_n$. The CQM extends this to terms like $\hat{a}_n^\dagger\hat{a}_m^\dagger$, $\hat{a}_n\hat{a}_m$, and $\hat{a}_n^\dagger\hat{a}_m$.

APPENDIX B: ENERGY CONSERVATION

To study the energy conservation, we consider the Hamiltonian

$$\hat{H} = \sum_{\sigma=\uparrow,\downarrow} \varepsilon_\sigma d_\sigma^\dagger d_\sigma + \sum_{\substack{\sigma=\uparrow,\downarrow \\ k\in L,R}} \varepsilon_k c_{k\sigma}^\dagger c_{k\sigma} + \sum_{\substack{\sigma=\uparrow,\downarrow \\ k\in L,R}} t_k d_\sigma^\dagger c_{k\sigma} + \text{h.c.}$$
$$+ U(n_\uparrow\theta(n_\downarrow - \Delta_\downarrow) + n_\downarrow\theta(n_\uparrow - \Delta_\uparrow)). \tag{B1}$$

This Hamiltonian is a close analog to what would be the constant of motion for the dynamics we employ. The contribution of the last term in the Hamiltonian to the equation of motion is given by

$$U(\{A, n_\uparrow\}\theta(n_\downarrow - \Delta_\downarrow) + \{A, n_\downarrow\}\theta(n_\uparrow - \Delta_\uparrow))$$
$$+U(\{A, \theta(n_\downarrow - \Delta_\downarrow)\}n_\uparrow + \{A, \theta(n_\uparrow - \Delta_\uparrow)\}n_\downarrow). \tag{B2}$$

The terms in the second line of Eq. (B2) are proportional to the Dirac delta function $\delta(n_\sigma - \Delta_\sigma)$ and are neglected in the dynamical map. In Fig. 6, we plot the ratio $\frac{|\langle\Delta H(t)\rangle|}{|\langle H(0)\rangle|}$, where $\Delta H(t) = H(t) - H(0)$. We find that the accumulated drift of the H is less than 0.05% of the total energy. We show this for both low and high temperatures and similar results were observed for small and large bias voltages.

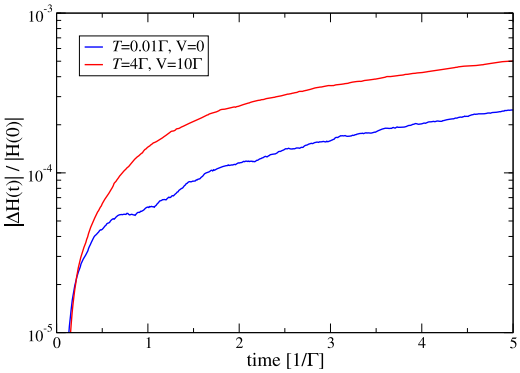

FIG. 6. The drift of the energy in time for different temperatures and source-drain voltages. The parameters are $U = 10\Gamma$, $\varepsilon = -5\Gamma$, and $\Gamma = 2\Gamma_L = 2\Gamma_R = 1$.

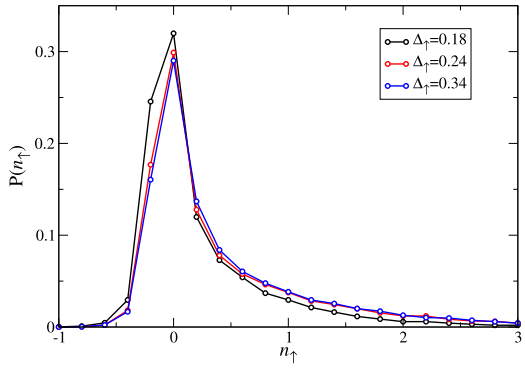

FIG. 7. The normalized distribution of the occupation number $n_\uparrow$ at steady-state, for different values $\Delta_\uparrow$. The distributions correspond to the data presented in Fig. 3 at the particle-hole symmetric point $\varepsilon = -5\Gamma$.

APPENDIX C: STEADY-STATE DISTRIBUTION OF THE OCCUPATION NUMBER

Figure 7 presents the normalized distribution of $n_\uparrow$ at steady-state. The three distributions correspond to the procedure of determining Δ_σ at the particle-hole symmetric point as explained in Sec. III C.

REFERENCES

[1] L. Mühlbacher and E. Rabani, Phys. Rev. Lett. **100**, 176403 (2008).
[2] S. Weiss, J. Eckel, M. Thorwart, and R. Egger, Phys. Rev. B **77**, 195316 (2008).
[3] M. Schiró and M. Fabrizio, Phys. Rev. B **79**, 153302 (2009).
[4] P. Werner, T. Oka, and A. J. Millis, Phys. Rev. B **79**, 035320 (2009).
[5] E. Gull, D. R. Reichman, and A. J. Millis, Phys. Rev. B **82**, 075109 (2010).
[6] D. Segal, A. J. Millis, and D. R. Reichman, Phys. Rev. B **82**, 205323 (2010).
[7] G. Cohen and E. Rabani, Phys. Rev. B **84**, 075150 (2011).
[8] R. Härtle, G. Cohen, D. Reichman, and A. Millis, Phys. Rev. B **88**, 235426 (2013).
[9] G. Cohen, E. Gull, D. R. Reichman, and A. J. Millis, Phys. Rev. Lett. **115**, 266802 (2015).
[10] P. Schmitteckert, Phys. Rev. B **70**, 121302 (2004).
[11] F. B. Anders and A. Schiller, Phys. Rev. Lett. **95**, 196801 (2005).
[12] R. Bulla, T. A. Costi, and T. Pruschke, Rev. Mod. Phys. **80**, 395 (2008).
[13] H. Wang and M. Thoss, Chem. Phys. **509**, 13 (2018).
[14] K. Balzer, Z. Li, O. Vendrell, and M. Eckstein, Phys. Rev. B **91**, 045136 (2015).
[15] L. Cao, V. Bolsinger, S. Mistakidis, G. Koutentakis, S. Krönke, J. Schurer, and P. Schmelcher, J. Chem. Phys. **147**, 044106 (2017).
[16] C. Schinabeck, A. Erpenbeck, R. Härtle, and M. Thoss, Phys. Rev. B **94**, 201407 (2016).
[17] E. Y. Wilner, H. Wang, G. Cohen, M. Thoss, and E. Rabani, Phys. Rev. B **88**, 045137 (2013).
[18] E. Y. Wilner, H. Wang, M. Thoss, and E. Rabani, Phys. Rev. B **90**, 115145 (2014).
[19] E. Y. Wilner, H. Wang, M. Thoss, and E. Rabani, Phys. Rev. B **89**, 205129 (2014).
[20] S. Datta, J. Phys.: Condens. Matter **2**, 8023 (1990).
[21] U. Harbola, M. Esposito, and S. Mukamel, Phys. Rev. B **74**, 235309 (2006).
[22] M. Leijnse and M. R. Wegewijs, Phys. Rev. B **78**, 235424 (2008).
[23] M. Esposito and M. Galperin, Phys. Rev. B **79**, 205303 (2009).
[24] M. Esposito and M. Galperin, J. Phys. Chem. C **114**, 20362 (2010).
[25] W. Dou, A. Nitzan, and J. E. Subotnik, J. Chem. Phys. **142**, 234106 (2015).
[26] A. Dorda, M. Ganahl, H. G. Evertz, W. von der Linden, and E. Arrigoni, Phys. Rev. B **92**, 125145 (2015).
[27] M. H. Hettler, J. Kroha, and S. Hershfield, Phys. Rev. B **58**, 5649 (1998).

[28] S. Datta, Superlattices Microstruct. **28**, 253 (2000).
[29] Y. Q. Xue, S. Datta, and M. A. Ratner, Chem. Phys. **281**, 151 (2002).
[30] M. Galperin, M. A. Ratner, and A. Nitzan, J. Phys.: Condens. Matter **19**, 103201 (2007).
[31] H. Haug and A.-P. Jauho, *Quantum Kinetics in Transport and Optics of Semiconductors*, Springer Series in Solid-State Sciences, 2nd ed. (Springer, Berlin, New York, 2008), pp. xix and 360.
[32] G. Stefanucci and R. v. Leeuwen, *Nonequilibrium Many-Body Theory of Quantum Systems: A Modern Introduction* (Cambridge University Press, 2013).
[33] H.-D. Mayer and W. H. Miller, J. Phys. Chem. **70**, 3214 (1979).
[34] W. H. Miller and K. A. White, J. Chem. Phys. **84**, 5059 (1986).
[35] T. Van Voorhis and D. R. Reichman, J. Chem. Phys. **120**, 579 (2004).
[36] W. H. Miller, J. Chem. Phys. **125**, 132305 (2006).
[37] D. W. Swenson, T. Levy, G. Cohen, E. Rabani, and W. H. Miller, J. Chem. Phys. **134**, 164103 (2011).
[38] D. W. Swenson, G. Cohen, and E. Rabani, Mol. Phys. **110**, 743 (2012).
[39] B. Li and W. H. Miller, J. Chem. Phys. **137**, 154107 (2012).
[40] B. Li, T. J. Levy, D. W. Swenson, E. Rabani, and W. H. Miller, J. Chem. Phys. **138**, 104110 (2013).
[41] B. Li, W. H. Miller, T. J. Levy, and E. Rabani, J. Chem. Phys. **140**, 204106 (2014).
[42] S. M. Davidson, D. Sels, and A. Polkovnikov, Ann. Phys. **384**, 128 (2017).
[43] A. Montoya-Castillo and T. E. Markland, Sci. Rep. **8**, 12929 (2018).
[44] U. Ray, G. K.-L. Chan, and D. T. Limmer, J. Chem. Phys. **148**, 124120 (2018).
[45] M. F. Herman and E. Kluk, Chem. Phys. **91**, 27 (1984).
[46] K. G. Kay, J. Chem. Phys. **101**, 2250 (1994).
[47] G. Stock and M. Thoss, Phys. Rev. Lett. **78**, 578 (1997).
[48] P. W. Anderson, Phys. Rev. **124**, 41 (1961).
[49] W. Miller and C. McCurdy, J. Chem. Phys. **69**, 5163 (1978).
[50] A. Levy, L. Kidon, J. Batge, J. Okamoto, M. Thoss, D. T. Limmer, and E. Rabani, J. Phys. Chem. C **123**, 13538 (2019).
[51] W. Dou, G. Miao, and J. E. Subotnik, Phy. Rev. Lett. **119**, 046001 (2017).